Kagome Lattice Promotes Chiral Spin Fluctuations

Kamil K. Kolincio[1,2,*,†] Max Hirschberger[1,3,*,‡] Jan Masell[1,4] Taka-hisa Arima[1,5]
Naoto Nagaosa,[1,3] and Yoshinori Tokura[1,3,6]

[1]*RIKEN Center for Emergent Matter Science (CEMS), Wako, Saitama 351-0198, Japan*
[2]*Faculty of Applied Physics and Mathematics, Gdańsk University of Technology, Narutowicza 11/12, 80-233 Gdańsk, Poland*
[3]*Department of Applied Physics and Quantum-Phase Electronics Center (QPEC),*
The University of Tokyo, Bunkyo-ku, Tokyo 113-8656, Japan
[4]*Institute of Theoretical Solid State Physics, Karlsruhe Institute of Technology (KIT), 76049 Karlsruhe, Germany*
[5]*Department of Advanced Materials Science, The University of Tokyo, Kashiwa 277-8561, Japan*
[6]*Tokyo College, The University of Tokyo, Bunkyo-ku, Tokyo 113-8656, Japan*

Dynamical spin fluctuations in magnets can be endowed with a slight bent toward left- or right-handed chirality by Dzyaloshinskii-Moriya interactions. However, little is known about the crucial role of lattice geometry on these chiral spin fluctuations and on fluctuation-related transport anomalies driven by the quantum-mechanical (Berry) phase of conduction electrons. Via thermoelectric Nernst effect and electric Hall effect experiments, we detect chiral spin fluctuations in the paramagnetic regime of a kagome lattice magnet; these signals are largely absent in a comparable triangular lattice magnet. Supported by Monte Carlo calculations, we identify lattices with at least two dissimilar plaquettes as most promising for Berry phase phenomena driven by thermal fluctuations in paramagnets.

Dynamical spin fluctuation processes, where large-scale chiral magnetic textures appear and decay as time passes, have become experimentally accessible to modern magnetism research with the rise of ultrafast optical and x-ray techniques, as well as diffuse small-angle neutron scattering [1–3]. It is now understood that such fluctuating, transient spin arrangements heavily impact the motion of conduction electrons in solids [4–8]. Consider, for simplicity, a single triangular cluster of three magnetic spins on lattice sites i, j, and k, where a chiral magnetic twist is imposed by spin-orbit interactions (Fig. 1). Theoretical work consistently shows that the time-averaged scalar spin chirality of the triangle, defined as $\chi = \langle \mathbf{S}_i \cdot (\mathbf{S}_j \times \mathbf{S}_k) \rangle$, can be finite and large even in the thermally disordered, paramagnetic state where $\langle \mathbf{S}_i \rangle \approx 0$ [4–9].

In terms of functional responses of solids, scalar spin chirality dictates the nature of moving electrons as quantum-mechanical waves, especially the geometrical phase of these waves (Berry phase) [10]. Each lattice plaquette passed by an electron wave packet adds a contribution $\sim \chi$ to its Berry phase [11–15], deflecting heat and charge currents [4–6,9], causing magneto-optical effects [16,17], and generating nonlinear processes such as the second harmonic generation of light [18]. Here, we move beyond previous experimental reports focused on the phenomenological observation of spin chirality generated by thermal fluctuations of spins [6,9,19]. Targeting the paramagnetic regime of a triangular lattice and a kagome lattice magnet, this Letter emphasizes structural geometry as a key factor in the amplification or suppression of lattice-averaged χ.

Our reference materials are $Gd_3Ru_4Al_{12}$ and Gd_2PdSi_3, metallic magnets with Néel temperatures of 18.6 and 21 K, respectively [20–24], and with highly similar magnetic phase diagrams featuring a skyrmion lattice phase [25,26]. Both materials crystallize in hexagonal structures—space group $P6_3/mmc$ and $P6/mmm$, respectively [27,28]—and the main building blocks of their magnetic sublattices are triangles of trivalent gadolinium ions, shown in Figs. 1(a) and 1(c). The spatial arrangement of these basic triangular units, however, constitutes a major difference between them: Gd_2PdSi_3's triangular lattice is a plain array of closely packed, edge-sharing, and identical triangles. Meanwhile, the magnetic spins in $Gd_3Ru_4Al_{12}$ are decorating a "breathing" kagome lattice, where alternating large and small triangles share corners with each other, being interspersed with hexagons [22]. As demonstrated here, this distorted kagome network is a model system for the exploration of spin chirality in thermal fluctuation processes.

Figure 1 illustrates how thermal fluctuations generate a net chiral habit in the paramagnetic state of solids. The high-temperature limit, depicted in Fig. 1(a), has spins fluctuating wildly in all directions of space. In this entirely random state, it is equally likely for a given spin triad to carry positive or negative $\langle \mathbf{S}_i \cdot (\mathbf{S}_j \times \mathbf{S}_k) \rangle$, even when a magnetic field is applied to break time-reversal symmetry. Upon cooling, short-range correlations develop and, on average, a single triangular unit may acquire finite chirality, see Fig. 1(b). Unbiased numerical calculations of the
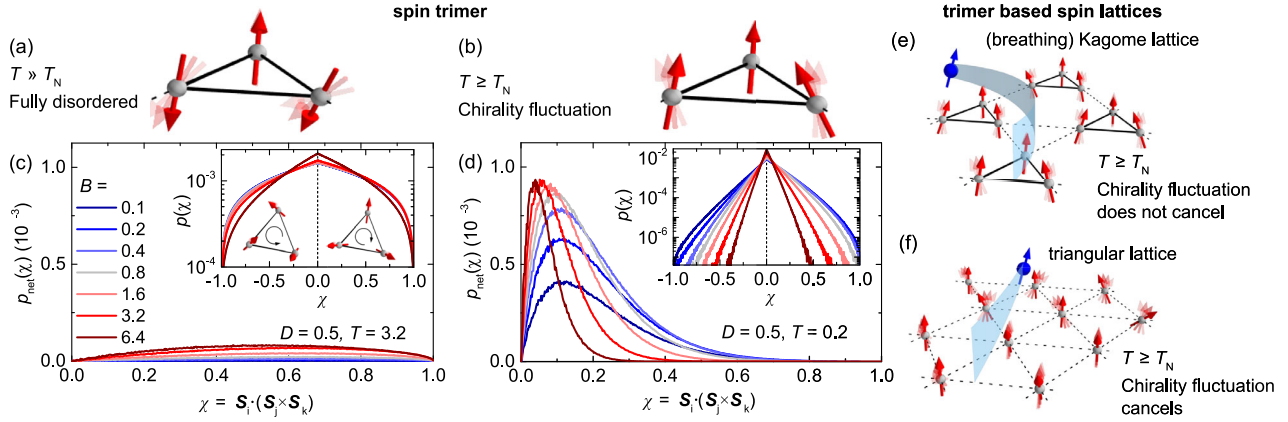
FIG. 1. Spin chirality and thermal fluctuations for lattices based on spin trimers. For a single triad of spins, we contrast (a) the fully disordered state with (b) a short-range correlated regime at lower temperature, with scalar spin chirality χ due to the influence of the Dzyaloshinskii-Moriya interaction D. (c) and (d): Antisymmetric part $p_{net}(\chi)$ (main panels) of the probability distribution $p(\chi)$ (inset) on a single triangle, from Monte Carlo simulations. B and T are the external magnetic field and temperature, respectively, expressed in units of the nearest-neighbor exchange interaction J. Cartoons: exemplary spin configurations with negative and positive χ. (e) and (f) The kagome lattice arrangement of spin trimers prevents cancellation of χ, while contributions from various triangles cancel for the triangular network.

high-temperature triad, detailed in the Supplemental Material [29], yield almost equal probability $p(\chi)$ for negative and positive spin chirality on a given triangle,

corresponding to a symmetric curve in the inset of Fig. 1(c), or to vanishingly small net probability $p_{net}(\chi) = p(\chi) - p(-\chi)$ in the main panel of Fig. 1(c).

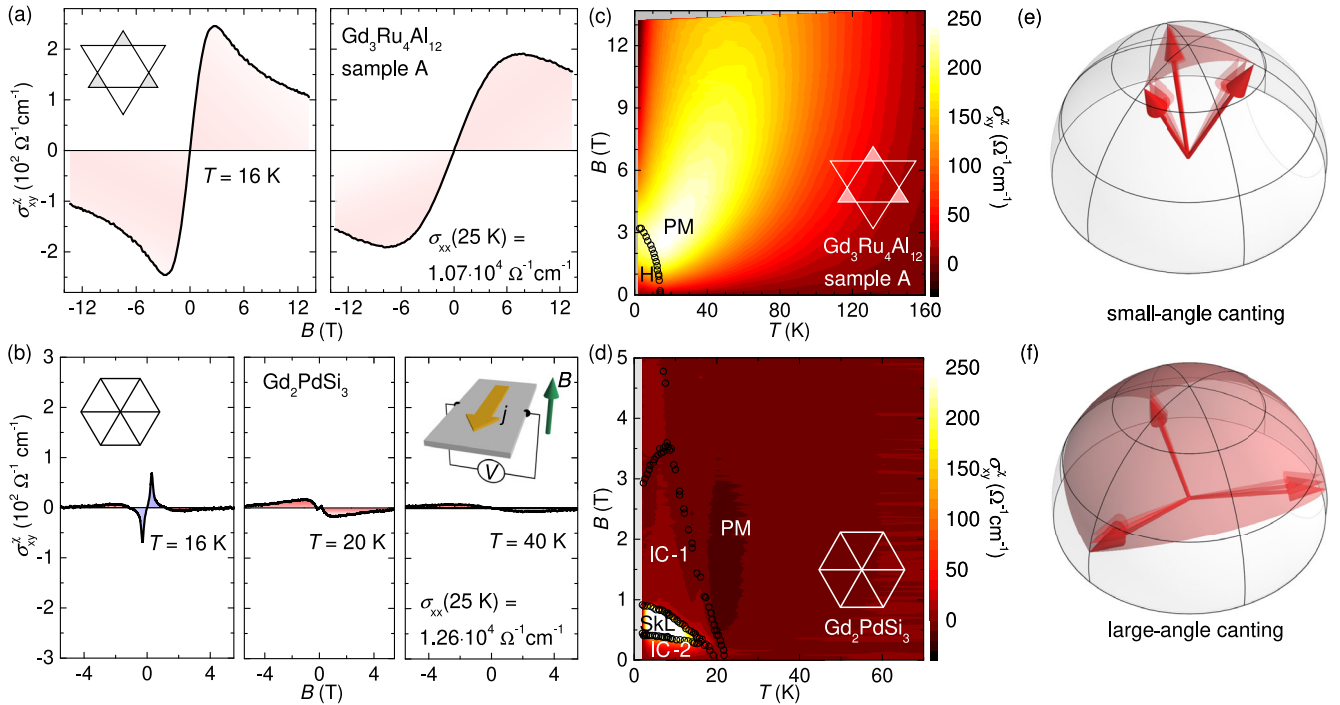FIG. 2. Chirality from spin fluctuations in transport experiments and dependence on lattice geometry. (a) and (b) Chirality-driven Hall effect σ_{xy}^{χ} in kagome lattice $Gd_3Ru_4Al_{12}$ and in triangular lattice Gd_2PdSi_3, below and above the ordering temperature T_N. Red (blue) shading corresponds to the fluctuating regime (the spin-ordered phase). Insets indicate the lattice type and measurement geometry. (c) and (d) Contour maps of σ_{xy}^{χ} in the plane spanned by magnetic field B and temperature T. The intensity scale is limited to 250 Ω^{-1} cm^{-1} and magnetic phases are labeled as PM (paramagnetic), H (helimagnetic order), IC (incommensurate magnetic order), and SkL (skyrmion lattice). (e) and (f) Small- and large-angle canting of a spin triad. Specifically, small-angle fluctuations cancel on trivial lattices, e.g., on the triangular grid. For a definition of trivial lattices, see Fig. 4.

We use the Hall conductivity σ_{xy} to detect the chirality of magnetic fluctuations. Sensing an effective sideways force on moving charges, the Hall effect has a contribution $\sim \int_{-\infty}^{\infty} d\chi\, p(\chi)\chi \sim \int_0^{\infty} d\chi\, p_{\mathrm{net}}(\chi)\chi$. At very high temperatures, instantaneous spin textures may have an imbalance of triangles with positive and negative local chirality, but there is no time- and lattice-averaged χ, and no net impact on conduction electron motion. As thermal agitation decreases and short-ranged spin-spin interactions become pronounced, even a weak external magnetic field causes unbalancing of $p(\chi)$. Figure 1(d) shows time-averaged local spin chirality and asymmetric probability distribution $p(\chi)$, so that the χ-driven Hall conductivity can become finite.

Depending on the lattice type, the chirality contribution σ_{xy}^{χ} to the Hall effect is amplified or strongly suppressed, illustrated in Figs. 1(e) and 1(f) for kagome and triangular lattices. Both structures are composed of triangle spin clusters, suitably described by our Monte Carlo calculations. Nonetheless, the presence of equivalent neighboring plaquettes causes cancellation of χ only for the triangular lattice [29].

Figures 2(a) and 2(c) present σ_{xy}^{χ} for the kagome system $Gd_3Ru_4Al_{12}$; the Supplemental Material explains how the chirality contribution is isolated from the raw data of Hall and Nernst effects [29]. Starting from zero magnetic field, the Hall signal rapidly increases: Even as spins are partially aligned, they retain the freedom to fluctuate around their average direction and to realize spin-chiral configurations. After attaining a maximum at intermediate fields, the Hall data drop when all spins are forcibly aligned. This behavior can be summarized in terms of a generic scaling between the magnetization and σ_{xy}^{χ} [19,29]. In the corresponding contour map of Fig. 2(c), the lattice-averaged spin chirality is already large deep inside the paramagnetic regime, further growing when cooling toward the magnetically ordered phase. From the standpoint of our numerical calculations [29] and of early theoretical work [4,5,39], this plume-shaped contour map emerges because lower and lower fields suffice to align all spins upon cooling. Note that σ_{xy}^{χ} can also be made to vanish at low temperature, when completely collinear spin alignment is realized by moderate magnetic fields.

The triangular lattice compound Gd_2PdSi_3 behaves quite differently: Its Hall signal σ_{xy}^{χ} in the paramagnetic regime is at least one order of magnitude smaller as compared to the kagome material $Gd_3Ru_4Al_{12}$ [Figs. 2(b) and 2(d)]. We propose that a significant suppression of the fluctuation-induced χ is rooted in the geometry of the triangular network: Here, each spin is shared between six equivalent triangles. While the weak canting of three next neighbors produces local spin chirality for an individual triad, contributions of neighboring triangles tend to have opposite sign. Integrating over the entire lattice plane, χ cancels to zero under the condition that the solid angle covered by fluctuations is small [29]. Large-amplitude spin fluctuations however, e.g., slowly fluctuating topological defects
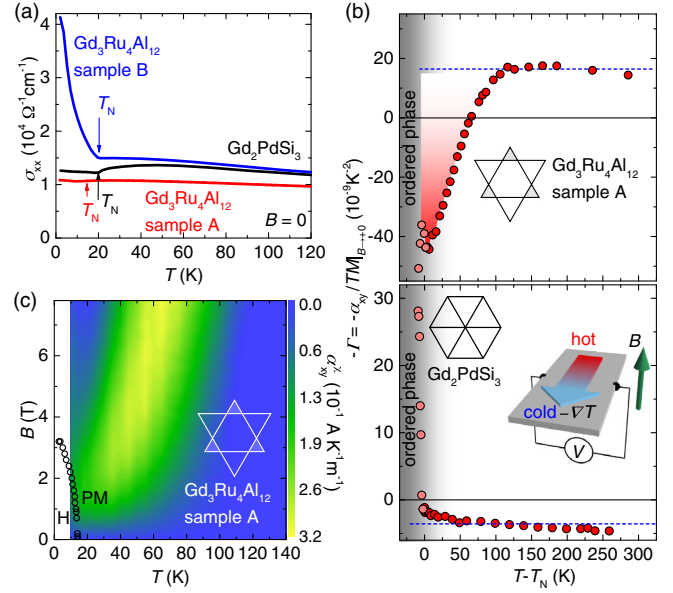

FIG. 3. Nernst effect from spin chirality in the paramagnetic regime. (a) Longitudinal conductivity σ_{xx}, demonstrating comparable metallicity for Gd_2PdSi_3 (black color) as well as samples A and B of $Gd_3Ru_4Al_{12}$ (red and blue color). (b) Thermoelectric Nernst conductivity divided by temperature and magnetization $\Gamma = \alpha_{xy}/(TM)|_{B\to+0}$, for kagome lattice (upper) and triangular lattice (lower). The long-range-ordered regime is marked by gray shading, and a dashed blue line indicates the anomalous Nernst effect proportional to the magnetization [29]. Inset: experimental geometry used for Nernst effect measurements [29]. (c) Thermoelectric Nernst conductivity α_{xy}^{χ} from thermal fluctuations, after subtraction of a background. Black circles indicate the boundary of the long-range-ordered state.

such as topological Z_2 vortices, skyrmions, and hedgehogs [14,40–42], escape from this extinction principle [Figs. 2(e) and 2(f)]. A small, yet finite chirality signal from thermal agitation can hence be created from large-angle fluctuations even on a simple triangular lattice [29].

On the kagome lattice of $Gd_3Ru_4Al_{12}$, $\sigma_{xy}^{\chi} \sim T^{-2}$ is observed to decay algebraically when heating at constant magnetic field, well described by an analytic high-temperature expansion of the spin chirality [29]. Our theoretical analysis confirms that Dzyaloshinskii-Moriya interactions underpin the observed fluctuation signal, ruling out spin chirality from anisotropic exchange interactions, single-ion compass anisotropy, and dynamically fluctuating, long-period spin textures [4,29]. We note that Hall and Nernst responses of materials with vastly different carrier relaxation times can hardly be compared quantitatively [43]. Figure 3(a) thus demonstrates comparable longitudinal electrical conductivity values σ_{xx} for Gd_2PdSi_3, $Gd_3Ru_4(Al_{0.95}Ga_{0.05})_{12}$ (sample A), and $Gd_3Ru_4Al_{12}$ (sample B).

Next, we use Fig. 3(b), inset, to introduce the experimental geometry for thermoelectric Nernst experiments: a transverse electric current J_y is driven by the applied temperature gradient $(-\nabla T)$, analogous to Hall's electric
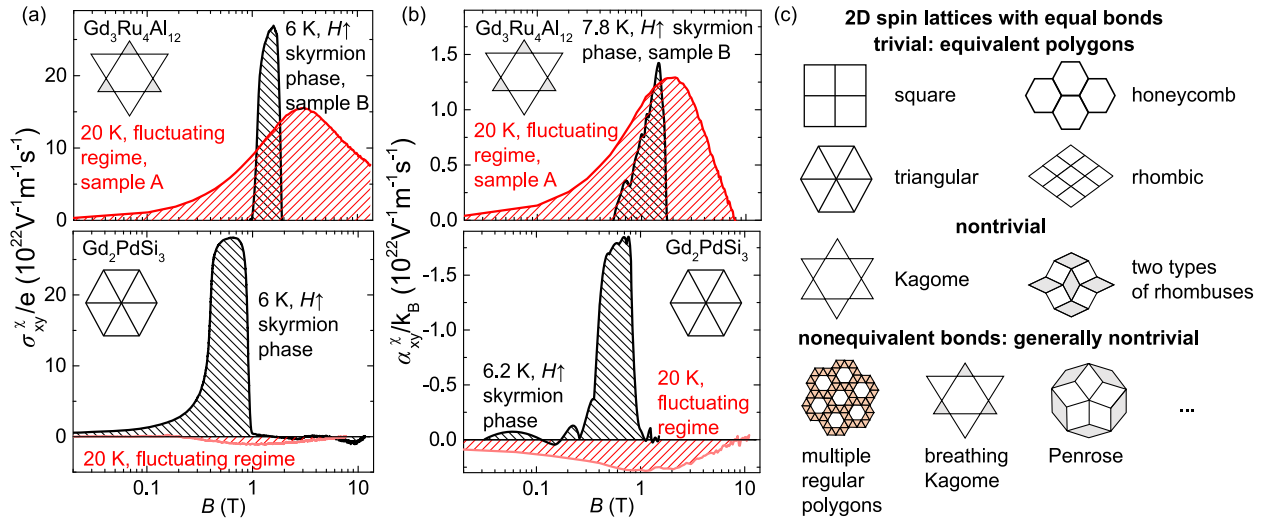
FIG. 4. Comparing static and fluctuation-driven spin chirality on triangular and kagome lattices. (a) and (b) Chirality-driven Hall conductivity σ_{xy}^{χ} (a) and Nernst conductivity α_{xy}^{χ} (b), with insets illustrating the lattice geometry. Black and red shading indicate signals in the static, long-range-ordered skyrmion lattice phase and spin-dynamic (fluctuating) paramagnetic regimes, respectively. (c) Classification of two-dimensional spin lattices as trivial and nontrivial, where trivial lattices cause cancellation of spin chirality between neighboring plaquettes. The grey shading of polygons is a guide to the eye and the three dots indicate a large number of additional nontrivial, two-dimensional lattices not depicted here.

current driven by an applied electric field. The thermoelectric Nernst conductivity α_{xy} includes a contribution from spin chirality, which is directly apparent in the ratio $\Gamma = \alpha_{xy}/(TM)|_{B\to+0}$: Fig. 3(b) demonstrates nearly temperature-independent behavior of this ratio for both compounds between room temperature and approximately 80 K. The high-temperature signal is the anomalous Nernst effect proportional to the net magnetization of the sample [29]. Below 80 K, a broad depression of said ratio appears only for the kagome lattice compound. This regime, where α_{xy} does not follow the magnetization even in the paramagnetic regime, marks the emergence of chiral spin fluctuations far above the transition to long-range order. In contrast, there is no clear Nernst anomaly for the triangular lattice, evidencing the suppression of χ on the simpler lattice type. A discussion of the sharply diverging data traces inside the ordered phases seen in Fig. 3(b) can be found in the Supplemental Material [29]. Summarizing the thermoelectric experiments, our contour map of the chirality-driven α_{xy}^{χ} of $Gd_3Ru_4Al_{12}$ is consistent with the Hall effect; in both cases, the signal appears at the boundary of the ordered phase and its plume deeply penetrates into the paramagnetic high-temperature state [Fig. 3(c)].

The present intermetallics are representative members of an emerging materials family hosting ultradense lattices of skyrmion spin-vortex tubes, with skyrmion diameter of only $\sim$2–3 nm [25,26,44,45]. In the skyrmion lattice, magnetic spins describe a 4π winding within each magnetic unit cell, hence providing a natural benchmark for the nonquantized spin chirality χ generated by thermal fluctuations. The skyrmion lattice of $Gd_3Ru_4Al_{12}$ produces a 1.4 $\times$ larger Hall effect than the maximal value realized by

thermal fluctuations in our experiments [Fig. 4(a), top]. As one magnetic skyrmion in $Gd_3Ru_4Al_{12}$ covers roughly 27 small triangles of the kagome network, Monte Carlo simulations predict 1.2 $\times$ larger lattice-averaged χ in the skyrmion lattice as compared to the fluctuating regime [29]. The reasonable agreement between experiment and this simple estimate justifies the choice of parameters in the numerical model. Meanwhile, σ_{xy}^{χ} and α_{xy}^{χ} in the paramagnetic state of Gd_2PdSi_3 [Fig. 4(a) and 4(a), top] are much suppressed as compared to the topological Hall and Nernst effects from the compound's skyrmion lattice [26,46] and also as compared to the fluctuation signals in $Gd_3Ru_4Al_{12}$ [Fig. 4(a) and (b), bottom]. Note that the Nernst and Hall signals in Fig. 4 are normalized by the Boltzmann constant k_B and the electric charge e, respectively. The Supplemental Material discusses the magnitude of these two signals in their fundamental units.

Having demonstrated a crucial role for lattice geometry in deciding the amplitude of σ_{xy}^{χ} and α_{xy}^{χ}, we may expand on our conclusions and offer a broader classification of planar tilings. Starting with lattices made from equilateral polygons, we define trivial lattice motifs as those where cancellation of χ occurs due to identical neighboring polygons. Of these, there are four basic types: square, triangular, and honeycomb lattices, assembled from regular polygons, as well as the rhombic tiling. Tiling motifs of the second group, labeled as nontrivial in Fig. 4(c), avoid cancellation due to the presence of at least two types of polygons. Among them, there are precisely two structures that have only one type of nearest-neighbor bond: the kagome lattice, and an arrangement of two rhombuses with dissimilar angles. For example, the kagome lattice avoids

cancellation of spin chirality by interspersing triangles with hexagons. Further relaxing the condition of equivalent bonds, a vast number of nontrivial, two-dimensional tiling motifs can be considered and realized in solids [47,48]; for example, the present breathing kagome structure of $Gd_3Ru_4Al_{12}$.

In summary, the implications of our Letter are not restricted to two-dimensional, periodic lattices: Quasi-layered sublattices of three-dimensional materials, for one, are amenable to such discussions. Consider the pyrochlore lattice of corner-sharing tetrahedra, a famous example from the field of frustrated magnetism: It features kagome layers when viewed along the cubic $\langle 111 \rangle$ direction. Moreover, quasicrystalline magnets, e.g., a Penrose tiling of rhombuses, are classified as nontrivial in our scheme. They are hence expected to generate large emergent responses in the paramagnetic state, when impressed with a fixed spin chirality by spin-orbit interactions, e.g., by the Dzyaloshinskii-Moriya coupling.

---

*These authors contributed equally to this work.

†kamil.kolincio@pg.edu.pl

‡hirschberger@ap.t.u-tokyo.ac.jp

[1] C. Pappas, E. Lelièvre-Berna, P. Falus, P. M. Bentley, E. Moskvin, S. Grigoriev, P. Fouquet, and B. Farago, Chiral Paramagnetic Skyrmion-like Phase in MnSi, Phys. Rev. Lett. **102**, 197202 (2009).

[2] F. Büttner, B. Pfau, M. Böttcher, M. Schneider, G. Mercurio *et al.*, Observation of fluctuation-mediated picosecond nucleation of a topological phase, Nat. Mater. **20**, 30 (2021).

[3] T. Shimojima, A. Nakamura, X. Yu, K. Karube, Y. Taguchi, Y. Tokura, and K. Ishizaka, Nano-to-micro spatiotemporal imaging of magnetic skyrmion's life cycle, Sci. Adv. **7**, eabg1322 (2021).

[4] W.-T. Hou, J.-X. Yu, M. Daly, and J. Zang, Thermally driven topology in chiral magnets, Phys. Rev. B **96**, 140403 (R) (2017).

[5] M. Böttcher, S. Heinze, S. Egorov, J. Sinova, and B. Dupé, $B - T$ phase diagram of Pd/Fe/Ir(111) computed with parallel tempering Monte Carlo, New J. Phys. **20**, 103014 (2018).

[6] W. Wang, M. W. Daniels, Z. Liao, Y. Zhao, J. Wang, G. Koster, G. Rijnders, C.-Z. Chang, D. Xiao, and W. Wu, Spin chirality fluctuation in two-dimensional ferromagnets with perpendicular magnetic anisotropy, Nat. Mater. **18**, 1054 (2019).

[7] H. Ishizuka and N. Nagaosa, Spin chirality induced skew scattering and anomalous Hall effect in chiral magnets, Sci. Adv. **4**, eaap9962 (2018).

[8] Y. Kato and H. Ishizuka, Colossal Enhancement of Spin-Chirality-Related Hall Effect by Thermal Fluctuation, Phys. Rev. Appl. **12**, 021001(R) (2019).

[9] K. Kolincio, M. Hirschberger, J. Masell, S. Gao, A. Kikkawaa, Y. Taguchi, T. h. Arima, N. Nagaosa, and Y. Tokura, Large Hall and Nernst responses from thermally induced spin chirality in a spin-trimer ferromagnet, Proc. Natl. Acad. Sci. U.S.A. **118**, e2023588118, (2021).

[10] M. V. Berry, Quantal phase factors accompanying adiabatic changes, Proc. R. Soc. A **392**, 45 (1984).

[11] J. Ye, Y. B. Kim, A. J. Millis, B. I. Shraiman, P. Majumdar, and Z. Tešanović, Berry Phase Theory of the Anomalous Hall Effect: Application to Colossal Magnetoresistance Manganites, Phys. Rev. Lett. **83**, 3737 (1999).

[12] G. Tatara and H. Kawamura, Chirality-driven anomalous Hall effect in weak coupling regime, J. Phys. Soc. Jpn. **71**, 2613 (2002).

[13] P. Bruno, V. K. Dugaev, and M. Taillefumier, Topological Hall Effect and Berry Phase in Magnetic Nanostructures, Phys. Rev. Lett. **93**, 096806 (2004).

[14] A. Neubauer, C. Pfleiderer, B. Binz, A. Rosch, R. Ritz, P. G. Niklowitz, and P. Böni, Topological Hall Effect in the A Phase of MnSi, Phys. Rev. Lett. **102**, 186602 (2009).

[15] R. Ritz, M. Halder, C. Franz, A. Bauer, M. Wagner, R. Bamler, A. Rosch, and C. Pfleiderer, Giant generic topological Hall resistivity of MnSi under pressure, Phys. Rev. B **87**, 134424 (2013).

[16] S. Sorn, L. Yang, and A. Paramekanti, Resonant optical topological Hall conductivity from skyrmions, Phys. Rev. B **104**, 134419 (2021).

[17] F. M. Bartram, S. Sorn, Z. Li, K. Hwangbo, S. Shen, F. Frontini, L. He, P. Yu, A. Paramekanti, and L. Yang, Anomalous Kerr effect in $SrRuO_3$ thin films, Phys. Rev. B **102**, 140408(R) (2020).

[18] H. Isobe, S.-Y. Xu, and L. Fu, High-frequency rectification via chiral Bloch electrons, Sci. Adv. **6**, eaay2497 (2020).

[19] Y. Lyanda-Geller, S. H. Chun, M. B. Salamon, P. M. Goldbart, P. D. Han, Y. Tomioka, A. Asamitsu, and Y. Tokura, Charge transport in manganites: Hopping conduction, the anomalous Hall effect, and universal scaling, Phys. Rev. B **63**, 184426 (2001).

[20] R. Mallik, E. Sampathkumaran, P. Paulose, H. Sugawara, and H. Sato, Magnetic anomalies in Gd_2PdSi_3, Physica (Amsterdam) **259-261B**, 892 (1999).

[21] V. Chandragiri, K. K. Iyer, and E. V. Sampathkumaran, Magnetic behavior of $Gd_3Ru_4Al_{12}$, a layered compound

with distorted kagomé net, J. Phys. Condens. Matter **28,** 286002 (2016).

[22] S. Nakamura, N. Kabeya, M. Kobayashi, K. Araki, K. Katoh, and A. Ochiai, Spin trimer formation in the metallic compound $Gd_3Ru_4Al_{12}$ with a distorted kagome lattice structure, Phys. Rev. B **98,** 054410 (2018).

[23] T. Matsumura, Y. Ozono, S. Nakamura, N. Kabeya, and A. Ochiai, Helical ordering of spin trimers in a distorted kagome lattice of $Gd_3Ru_4Al_{12}$ studied by resonant x-ray diffraction, J. Phys. Soc. Jpn. **88,** 023704 (2019).

[24] S. Spachmann, A. Elghandour, M. Frontzek, W. Löser, and R. Klingeler, Magnetoelastic coupling and phases in the skyrmion lattice magnet Gd_2PdSi_3 discovered by high-resolution dilatometry, Phys. Rev. B **103,** 184424 (2021).

[25] M. Hirschberger, T. Nakajima, S. Gao, L. Peng, A. Kikkawa, T. Kurumaji, M. Kriener, Y. Yamasaki, H. Sagayama, H. Nakao, K. Ohishi, K. Kakurai, Y. Taguchi, X. Yu, T.-h. Arima, and Y. Tokura, Skyrmion phase and competing magnetic orders on a breathing kagomé lattice, Nat. Commun. **10,** 5831 (2019).

[26] T. Kurumaji, T. Nakajima, M. Hirschberger, A. Kikkawa, Y. Yamasaki, H. Sagayama, H. Nakao, Y. Taguchi, T.-h. Arima, and Y. Tokura, Skyrmion lattice with a giant topological Hall effect in a frustrated triangular-lattice magnet, Science **365,** 914 (2019).

[27] P. A. Kotsanidis, J. K. Yakinthos, and E. Gamari-Seale, Magnetic properties of the ternary rare earth silicides R_2PdSi_3 ($R =$ Pr, Nd, Gd, Tb, Dy, Ho, Er, Tm and Y), J. Magn. Magn. Mater. **87,** 199 (1990).

[28] R. E. Gladyshevskii, O. R. Strusievicz, K. Cenzual, and E. Parthé, Structure of $Gd_3Ru_4Al_{12}$, a new member of the $EuMg_{5.2}$ structure family with minority-atom clusters, Acta Crystallogr. Sect. B **49,** 474 (1993).

[29] See Supplemental Material at http://link.aps.org/supplemental/10.1103/PhysRevLett.130.136701 for detailed descriptions of used materials and methods as well as the theoretical calculations, which also includes Refs. [30–38].

[30] S. R. Saha, H. Sugawara, T. D. Matsuda, H. Sato, R. Mallik, and E. V. Sampathkumaran, Magnetic anisotropy, first-order-like metamagnetic transitions, and large negative magnetoresistance in single-crystal Gd_2PdSi_3, Phys. Rev. B **60,** 12162 (1999).

[31] F. Tang, M. Frontzek, J. Dshemuchadse, T. Leisegang, M. Zschornak, R. Mietrach, J.-U. Hoffmann, W. Löser, S. Gemming, D. C. Meyer, and M. Loewenhaupt, Crystallographic superstructure in R_2PdSi_3 compounds ($R =$ heavy rare earth), Phys. Rev. B **84,** 104105 (2011).

[32] L. Spitz, T. Nomoto, S. Kitou, H. Nakao, A. Kikkawa, S. Francoual, Y. Taguchi, R. Arita, Y. Tokura, T. h. Arima, and M. Hirschberger, Entropy-assisted, long-period stacking of Honeycomb layers in an AlB_2-type silicide, J. Am. Chem. Soc. **144,** 16866 (2022).

[33] S. Grytsiuk, J.-P. Hanke, M. Hoffmann, J. Bouaziz, O. Gomonay, G. Bihlmayer, S. Lounis, Y. Mokrousov, and S. Blügel, Topological-chiral magnetic interactions driven by emergent orbital magnetism, Nat. Commun. **11,** 511 (2020).

[34] J. Kindervater, I. Stasinopoulos, A. Bauer, F. X. Haslbeck, F. Rucker, A. Chacon, S. Mühlbauer, C. Franz, M. Garst, D. Grundler, and C. Pfleiderer, Weak Crystallization of Fluctuating Skyrmion Textures in MnSi, Phys. Rev. X **9,** 041059 (2019).

[35] M. Raju, A. P. Petrović, A. Yagil, K. S. Denisov, N. K. Duong, B. Göbel, E. Şaşıoğlu, O. M. Auslaender, I. Mertig, I. V. Rozhansky, and C. Panagopoulos, Colossal topological Hall effect at the transition between isolated and lattice-phase interfacial skyrmions, Nat. Commun. **12,** 2758 (2021).

[36] F. Izumi and K. Momma, Three-dimensional visualization in powder diffraction, Solid State Phenom. **130,** 15 (2007).

[37] M. Hirschberger, T. Nakajima, M. Kriener, T. Kurumaji, L. Spitz, S. Gao, A. Kikkawa, Y. Yamasaki, H. Sagayama, H. Nakao, S. Ohira-Kawamura, Y. Taguchi, T.-h. Arima, and Y. Tokura, High-field depinned phase and planar Hall effect in the skyrmion host Gd_2PdSi_3, Phys. Rev. B **101,** 220401(R) (2020).

[38] L. Xu, X. Li, L. Ding, T. Chen, A. Sakai, B. Fauqué, S. Nakatsuji, Z. Zhu, and K. Behnia, Anomalous transverse response of Co_2MnGa and universality of the room-temperature $\alpha_{ij}^A/\sigma_{ij}^A$ ratio across topological magnets, Phys. Rev. B **101,** 180404(R) (2020).

[39] L. Rózsa, E. Simon, K. Palotás, L. Udvardi, and L. Szunyogh, Complex magnetic phase diagram and skyrmion lifetime in an ultrathin film from atomistic simulations, Phys. Rev. B **93,** 024417 (2016).

[40] M. Lau and C. Dasgupta, Role of topological defects in the phase transition of the three-dimensional Heisenberg model, J. Phys. A **21,** L51 (1988).

[41] B. Binz and A. Vishwanath, Chirality induced anomalous-Hall effect in helical spin crystals, Physica (Amsterdam) **403B,** 1336 (2008).

[42] H. Kawamura, A. Yamamoto, and T. Okubo, Z_2-vortex ordering of the triangular-Lattice Heisenberg antiferromagnet, J. Phys. Soc. Jpn. **79,** 023701 (2010).

[43] N. Nagaosa, J. Sinova, S. Onoda, A. H. MacDonald, and N. P. Ong, Anomalous Hall effect, Rev. Mod. Phys. **82,** 1539 (2010).

[44] T. Okubo, S. Chung, and H. Kawamura, Multiple-q States and the Skyrmion Lattice of the Triangular-Lattice Heisenberg Antiferromagnet under Magnetic Fields, Phys. Rev. Lett. **108,** 017206 (2012).

[45] N. D. Khanh, T. Nakajima, X. Yu, S. Gao, K. Shibata, M. Hirschberger, Y. Yamasaki, H. Sagayama, H. Nakao, L. Peng, K. Nakajima, R. Takagi, T. h. Arima, Y. Tokura, and S. Seki, Nanometric square skyrmion lattice in a centrosymmetric tetragonal magnet, Nat. Nanotechnol. **15,** 444 (2020).

[46] M. Hirschberger, L. Spitz, T. Nomoto, T. Kurumaji, S. Gao, J. Masell, T. Nakajima, A. Kikkawa, Y. Yamasaki, H. Sagayama, H. Nakao, Y. Taguchi, R. Arita, T.-H. Arima, and Y. Tokura, Topological Nernst Effect of the Two-Dimensional Skyrmion Lattice, Phys. Rev. Lett. **125,** 076602 (2020).

[47] R. Williams, *The Geometrical Foundation of Natural Structure. A Source Book of Design* (Dover Publications, New York, 1979).

[48] A. Holden, *Shapes, Space, and Symmetry* (Columbia University Press, New York, 1971).